Measurements of Nearshore Waves through Coherent Arrays of Free-Drifting Wave Buoys

Edwin Rainville[1], Jim Thomson[1,*], Melissa Moulton[1,2,*], and Morteza Derakhti[1,*]

[1]University of Washington - Applied Physics Laboratory, Air-Sea Interaction, Seattle, WA 98105, USA
[2]National Center for Atmospheric Research, Boulder, CO 80305, USA
[*]these authors contributed equally to this work

Correspondence: Edwin Rainville (erainvil@uw.edu)

Abstract. Along coastlines, surface gravity wave breaking occurs in complex spatial and temporal patterns that significantly impact erosion, scalar transport, and flooding. Numerical models are used to predict these processes, but many models lack sufficient evaluation with observations during storm events. To fill the need for more nearshore wave measurements during extreme conditions, we deployed coherent arrays of small-scale, free-drifting wave buoys named microSWIFTs. The result

5   is a large dataset covering a range of conditions. The microSWIFT is a small wave buoy equipped with a GPS module and Inertial Measurement Unit (IMU) used to directly measure the buoy's global position, horizontal velocities, rotation rates, accelerations, and heading. We use an Attitude and Heading Reference System (AHRS), 9 degrees-of-freedom Kalman filter to rotate the measured accelerations from the reference frame of the buoy to the Earth reference frame. We then use the corrected accelerations to compute the vertical velocity and sea surface elevation. The measurements were collected over a 27-day field

10   experiment in October of 2021 at the US Army Corps of Engineers Field Research Facility in Duck, NC. The microSWIFTs were deployed as a series of coherent arrays, meaning they all sampled simultaneously with a common time reference, leading to a robust spatial and temporal dataset during each deployment. We evaluate wave spectral energy density estimates from individual microSWIFTs by comparing them with a nearby acoustic waves and currents (AWAC) sensor. We also compare significant wave height estimates from the coherent arrays with the nearby AWAC estimates. A zero crossing algorithm is

15   applied to each buoy time series of sea surface elevation to extract realizations of measured surface gravity waves, yielding 116,307 wave realizations throughout the experiment. These measurements spanned offshore significant wave heights ranging from 0.5 meters to 3 meters and peak wave periods ranging from 5 to 15 seconds over the entire experiment. These data are available at https://doi.org/10.5061/dryad.hx3ffbgk0 (Rainville et al., 2023) and will be used as a validation dataset for wave-averaged and wave-resolving models and will be used to investigate nearshore wave dynamics.

20   1   Introduction

The ocean covers most of the surface of the Earth, and by 2002 about 41% of the people on Earth live within 100 km of the coast; we expect this population has continued growing (Boehm et al., 2017; Martínez et al., 2007). We expect sea levels to rise and storm frequency and intensity to increase due to climate change, making coastlines more susceptible to flooding, infrastructure damage, and loss of life (Intergovernmental Panel on Climate Change, 2021). Under moderate greenhouse gas

emission forcing scenarios, we predict approximately \$990 billion in damages to US coastlines between now and the year 2100 due to storm surge and sea level rise (Neumann et al., 2015). Wave forcing is a significant component of the total storm surge that causes flooding in low-lying coastal areas (Bertin, 2016). As surface gravity waves propagate towards the shore, they also transport energy and momentum, which drives nearshore circulation and scalar transport (Svendsen, 2005). Understanding and quantifying the dissipation of wave energy can improve our understanding of circulation and transport patterns which are essential for proper coastal management. Operational wave forecast models that predict nearshore wave transformation do not resolve individual waves and instead use a spectral representation of the waves in models such as SWAN (Simulating Waves Nearshore, (Booij et al., 1996)) and WWIII (Wave Watch III, (Tolman, 1999)). Other wave models are wave-resolving, such as NHWAVE (Derakhti et al., 2016a; Ma et al., 2012) and FUNWAVE (Kirby et al., 1998; Shi et al., 2012), but are computationally expensive and therefore are not used operationally. Since the operational models do not resolve individual waves, they do not resolve individual wave processes, such as wave breaking. Therefore, to represent these processes in the operational models, we must parameterize them. Individual wave breaking has been investigated in wave-resolving models in Derakhti et al. (2016a) and Derakhti et al. (2016b). However, implementing these processes to wave-averaged models still needs to be explored further. A dataset with both wave-resolved and wave-averaged measurements is required to investigate the wave-averaged model parameterizations for individual wave processes.

Fixed sensors, such as acoustic waves and currents (AWAC) meters, are used to measure time series of wave parameters such as significant wave height and mean wave period. Fixed sensors generally have robust statistics since they measure continuously for long periods. However, it is challenging to deploy and maintain fixed sensors in the harsh surf-zone environment, and these logistics and sensor costs can limit the number of sensors deployed. As an alternative to fixed sensors, wave buoys have become the best option for studying a wide variety of sea states with a specific emphasis on extreme events. Free-drifting buoys tend to move through the surf zone very quickly and, therefore, to have comparable statistics to the fixed sensors, multiple buoys are deployed simultaneously. These simultaneously deployed buoys are known as coherent arrays of buoys. They are used to improve the robustness of individual buoy measurements and show the spatial variation of the wave field.

Early wave buoys used measurements of the buoy's heave, pitch, and roll to compute the scalar and directional energy spectra (Kuik et al., 1988). The next generation of wave buoys, including the SWIFT (Surface Wave Instrumentation Floats with Tracking) buoy, focused on using GPS velocity-based processing methods. GPS-based wave buoys have been effective at measuring deep water ocean waves; however, they are limited to measuring deep water waves due to an implicit assumption of circular wave orbital motion (Thomson, 2012). GPS-based processing also facilitated smaller-scale and more cost-effective wave buoys with comparable accuracy in their estimates of energy density spectra and bulk wave parameters to fixed platforms (Thomson et al., 2018; Herbers et al., 2012). GPS-based drifters have also been used to investigate surf-zone dispersion and circulation patterns (Schmidt et al., 2003, 2005; Spydell et al., 2007).

There are now many small, GPS-based wave buoys in common usage. SWIFT buoys have been used to measure turbulence (Thomson, 2012; Thomson et al., 2016), wave-ice interactions (Voermans et al., 2019) and wave-current interactions (Zippel and Thomson, 2017). SWIFTs have also been used to quantify the breaking severity of individual waves (Brown et al., 2019). The company *SOFAR ocean* has since developed the Spotter buoy that uses a GPS-based wave measurement. Many Spotter

60 buoys are deployed worldwide to create a global network of wave measurements that can be assimilated into a global wave model and thus assist industries reliant on accurate forecasts of waves (Raghukumar et al., 2019). The significant improvements in individual buoys over recent decades have made it possible to deploy large numbers of buoys and process these simultaneously to improve spatial resolution and statistical robustness of measurements.

In the following sections, we discuss the development of the microSWIFT wave buoy (Section 2.2), the deployment of
65 microSWIFTs as part of the During Nearshore Events Experiment (DUNEX) (Section 2.2), the creation of a large dataset including raw and post-processed measurements (Section 2.3), and the utility of that dataset for studying nearshore waves and circulation (Section 3).

2   Data Collection - During Nearshore Event Experiment (DUNEX)

This project is part of a larger collaborative effort called DUNEX (During Nearshore Event Experiment) that is funded through
70 the US Coastal Research Program (USCRP, https://uscoastalresearch.org). The overall goal of DUNEX is to use rapid-response or other event-focused measurements and models to improve understanding of coastal impacts during storm events, when historically it has been difficult to make measurements. As a part of DUNEX, a 27-day field experiment was held from October 3-30, 2021. During the field experiment, our team contributed to the overall DUNEX effort by measuring the motion of small-scale, free-drifting microSWIFT buoys in the inner shelf and surf zone. The microSWIFTs move with the free surface, thus
75 providing measurements of surface waves and mass transport. The following subsections will describe the data collection from DUNEX, including the field experiment, microSWIFT development, and data processing.

2.1   Field Experiment Site and Conditions - US Army Corps of Engineers Field Research Facility (FRF)

The experiment was conducted at the US Army Corps of Engineers (US-ACE) Field Research Facility (FRF) in Duck, North Carolina, USA (Figure 1). This site has a long history of being the focus of coastal dynamics experiments and is a relatively
80 well-understood energetic sandy beach environment (Elgar et al., 1997; Gallagher et al., 1998; Feddersen et al., 1998). The site maintains long-term observations via fixed in situ instrumentation, regular bathymetric surveys, remote sensing camera, and LiDAR measurements. The detailed and frequent bathymetric surveys were essential to the study, as the bathymetry in the nearshore ocean is one of the dominant controls on local hydrodynamics (Svendsen, 2005). The FRF has an established local Cartesian coordinate system with a cross-shore position $x = 200$ near the mean shoreline position, increasing offshore, and
85 $y = 500$ at the location of the pier in the middle of the study site, increasing northward. The bathymetry typically includes a large shore-perpendicular channel at approximately 500 meters in the alongshore direction underneath the pier due to scour. During the October 2021 study time period, a long shore-parallel sandbar at approximately 200 meters in the cross-shore direction and changed on timescales of hours to days (Ruessink et al., 2001).

A cross-shore transect of instruments near $y = 900$ maintained by the FRF includes several sensors in and near the surf zone
90 that are relevant to this study. This sensor array includes a Nortek Acoustic Waves and Currents (AWAC) sensor in 4.5-m mean water depth, another AWAC in 6-m mean depth, and an array of pressure gauges in 8-m depth used to estimate wave-directional

spectra (Figure 1, Panel B). These sensors recorded the measurements of surface gravity waves during the experiment and are processed to give estimates of the bulk parameters of significant wave height, mean wave period, and mean wave direction for the duration of the field experiment (Figure 2). During the experiment, significant wave heights ranged from 0.5 to 3 meters,

95   mean wave periods from 5 to 15 seconds, and mean wave directions from 20 to 120 degrees relative to true North (where the cross shore normal direction is 71.8 degrees clockwise of true North). We were able to sample during most of the various conditions, giving us an extensive range of conditions.

2.2   microSWIFT Buoy Development and Deployments

The microSWIFT buoys are named after their predecessor, the SWIFT buoy (Thomson, 2012). The electronics and sensors of
100   the microSWIFT are housed inside a Nalgene-brand water bottle with a length of 21 cm and a diameter of 9 cm (Figure 3). The bottle sits on its side in the water, giving a keel of 4.5 cm and a sail of 4.5 cm. The overall microSWIFT has a mass of 0.7 kg. It is powered by two rechargeable lithium-iron D-cell batteries and has an approximate lifespan of 48 hours under the current operating configuration. The instruments on board the microSWIFT are a GPS module and Inertial Measurement Unit (IMU). A Raspberry Pi Zero, a small microprocessor with a Raspian Linux operating system, controls the entire system. The
105   microSWIFT also has an iridium modem (RockBLOCK 9603) onboard that sends processed data from the microSWIFT to a shore-side server. Each component of the microSWIFT is soldered directly onto a custom circuit board (Figure 3). This is version 1 of the microSWIFT.

All software for the microSWIFT is written in the Python computing language and is published on a public Github repository for open source access (https://github.com/SASlabgroup/microSWIFT). The flow of onboard software is shown in Figure 4.
110   The microSWIFT is controlled by one primary function named *microSWIFT.py* that controls all other functions. When the microSWIFT boots up, a service script named *microSWIFT.service* runs and starts the main *microSWIFT.py* control function. As *microSWIFT.py* starts, it creates a log file where all functions onboard the microSWIFT are logged so the user can see if any errors are occurring or if the instrument is working correctly. The microSWIFT central control is split into two windows, the record and process/send windows, with user-defined lengths based on universal coordinated time (UTC). Within the record
115   window, the microSWIFT concurrently records GPS and IMU data and writes the data directly to a file. The microSWIFT enters the process/send window when the record window ends. Here, the microSWIFT reads in all of the recorded GPS velocities and uses the algorithm *GPSwaves* described in Thomson (2012); Thomson et al. (2018) to compute an estimate of the wave energy scalar spectrum, bulk parameters, last known location, and the average north-south and east-west velocities over the length of the last record window. These processed values are then packaged into a binary message sent through the iridium modem to
120   a shore-side server where the data can be parsed and used. The *GPSwaves* algorithm is very effective for deep water waves; however, it uses an assumption of circular wave orbital velocities to estimate the scalar energy spectrum. The elliptical orbits of shoaling waves in shallow water violate this assumption. The nonlinearity of breaking waves further complicates the usage of GPS velocities to infer wave elevations. For nearshore applications, we developed a new processing method described in Section 2.3.

125   As the microSWIFT drifts, the IMU and GPS sensors measure the motion of the bottle. The IMU measures accelerations, rotation rates, and magnetic heading in three orthogonal spatial dimensions at a rate of 12 Hz in the reference frame of the buoy. The chipsets, sensitivities, and ranges of the accelerometer, gyroscope, and magnetometer are shown in Table 1. The GPS receiver is an MT3339 chipset that samples at a rate of 4 Hz and measures latitude, longitude, altitude, and horizontal velocities in the Earth reference frame. These measurements provide a comprehensive picture of how and where each microSWIFT moves
130 in response to waves and surface currents.

    Each microSWIFT provides detailed information about a single point in space and time. However, when deployed in large numbers as coherent arrays, the microSWIFTs can be processed together to explore the spatial variability of the nearshore waves and currents. The deployed coherent arrays ranged in size from two to fifty microSWIFTs, either in an alongshore line outside of the surf zone or in a cross-shore line extending from outside of the surf zone onshore into the surf zone. Our team
135 deployed the buoys by throwing them from the pier, paddling them out on surfboards, dropping them from a helicopter, or providing them to local lifeguards who dropped them off a jetski. The microSWIFTs were retrieved when they eventually washed up on the beach or were chased down using surfboards, jet skis, and boats. We refer to each deployed array as a "mission." Drift tracks (location of each microSWIFT over the time of a mission) from the microSWIFTs on two example missions are shown in Figure 5. After data cleaning, the dataset consists of 68 missions spanning 27 days.

140 **2.3   Data Levels and Data Processing**

We separate three levels of data as follows:

- Level 0: Text files of raw data from the GPS and IMU from each microSWIFT, organized by the mission number

- Level 1: GPS and IMU measurements stored in a netCDF file, data have been cleaned and interpolated onto the same time datum for each mission

145   - Level 2: IMU accelerations that have been corrected to the Earth frame of reference, with velocities and positions computed from these corrected accelerations

    First, we download the Level 0 raw measurements from the microSWIFTs, organize them into folders for each mission, then read the data from the text files. We then create a single time array with the mission's manually recorded start and end times. The start time is when all the microSWIFTs entered the water, and the end time is when all the microSWIFTs are out of the
150 water. The time step in this time array matches the IMU sample rate of 12 Hz. We then match the IMU measurements to this time array and linearly interpolate the GPS data to match the time array. Any gaps in the IMU measurements are filled with linear interpolation. Gaps are rare; typically, no points are missing.

    We then clean these data using a combination of automated and manual methods. First, we create a spatial threshold to remove data points while a microSWIFT is on the beach. We create this threshold using a digital elevation model of the
155 bathymetry at the FRF from October 21st, 2021 (elevation is relative to NAVD88) (Figure 1, Panel (b)) and the mean water level during each mission measured by a NOAA tide gauge (Location in Figure 1, Panel (b)). The mean water level is added to

the bathymetry measurements to find the depth at each surveyed point during each mission. We find the furthest offshore dry point as the furthest offshore positive value. We then add a buffer of two additional meters to the furthest offshore dry point and set this location as the spatial threshold for that mission. We replaced any points that cross this beach threshold on the beach side with "NaN" values in the dataset. While there were changes in the bathymetry during the experiment, we are only using this survey to define an approximate location of the beach extent to do a bulk data cleaning. After this automated cleaning method, we manually inspected each data channel for any spurious points that were also replaced with "NaN" values.

The recorded start and end times of the mission were also manually adjusted to reflect the times the microSWIFTs were actually in the water. Large spikes in acceleration at the beginning of a deployment tend to represent times when the start time was recorded too early and was adjusted to remove these spikes. Similarly, the microSWIFTs were sometimes picked up in the middle of the mission, e.g., during jetski-based deployments, and those times were manually removed as well. All data cleaning, including start and end time adjustment and individual point cleaning, is noted in Appendix B in Rainville et al. (2022), and the cleaning notes are stored in the metadata of each netCDF and in the GitHub repository that contains all processing code (https://github.com/SASlabgroup/DUNEXMainExp). The IMU data is then despiked using a piecewise cubic Hermite interpolating polynomial (PCHIP) function, a shape-preserving interpolation scheme used to reduce overshoot oscillations and maintain continuity (Karim et al., 2014). Points with a value greater than four scaled median absolute deviations from the median are considered outliers and replaced using the PCHIP method. The cleaned and despiked dataset is considered the Level 1 data.

We use the gyroscope and magnetometer measurements to correct the accelerations from the body reference frame to the Earth reference frame using a 9 degrees-of-freedom indirect Kalman filter for IMU sensor fusion that is prepackaged in the MATLAB navigation toolbox (MATLAB Navigation Toolbox 2022b, https://www.mathworks.com/help/nav/multisensor-positioning.html). A schematic representation and an example corrected signal are shown, respectively, in Panels (a) and (b) of Figure 6. The corrections to the acceleration are generally minor (see changes between uncorrected and corrected vertical acceleration in Figure 6, Panel (b)) but have a significant impact on the integrated signals and eventually computed energy spectra and bulk wave parameters. The essential acceleration component is vertical, integrated in time to estimate vertical velocity and integrated again to estimate sea surface elevation. We then use a first-order Butterworth band-pass filter to remove low ($f < 0.05$ Hz) and high ($f > 0.5$ Hz) frequency noise outside of the gravity wave band from the signals. We then integrate the filtered acceleration signals via a time domain cumulative trapezoid method to velocities. The velocities are then filtered again with the same filter to eliminate any spurious integration errors, then integrated to estimate positions, and finally filtered one last time to eliminate integration errors. The corrected and filtered accelerations, velocities, and positions are the Level 2 data.

3 Evaluation of microSWIFTs and microSWIFT Arrays

To assess the reliability of this dataset and the new microSWIFT wave buoys, we compared the wave measurements from the microSWIFTs to measurements from a Nortek Acoustic Waves and Current (AWAC) sensor that is mounted to the seafloor at a

190   nominal depth of 4.5 meters at the field site (referred to as the 4.5 m AWAC, location in Figure 1, Panel (b)). The 4.5 m AWAC is currently at a bottom elevation of -4.8 meters relative to NAVD88 due to changes in the bathymetry since the instrument was initially deployed and named. The AWAC estimates the scalar energy spectrum and bulk wave parameters which we will use as ground truth to compare with estimates from the microSWIFTs. AWAC sensors have been validated for use in the nearshore environment in prior studies (Pedersen et al., 2007). Known limitations of the AWAC include excess noise at high frequencies

195   and reduced response at low frequencies.

To evaluate individual microSWIFT measurements, we compare the energy density spectra estimated from the 4.5 m AWAC and individual microSWIFTs. We assume that the main control of nearshore wave evolution is the local bathymetry, and therefore measurements in similar depths at the same time should be comparable in a spectral and statistical framework (Gomes et al., 2016). However, we expect some differences since the measurements are at different locations. To compute an energy

200   spectral density estimate from an individual microSWIFT that we can compare to the 4.5 m AWAC, we use data when an individual microSWIFT was at a location that corresponded to a bottom elevation between -4.3 and -5.3 ($\pm$ 0.5 meters around the current elevation of the AWAC) meters based on the local bathymetry measurements in Figure 1, Panel (b). We find that mission 18 has four microSWIFTs that were between these depths for almost 10 consecutive minutes as they drifted through the surf zone (Figure 7, Panels (a) and (b)). The spectra are computed using Welch's method, with Hanning windows of 300

205   seconds(3600 points) long and 50% overlap between adjacent windows. The energy in each five adjacent frequencies are band-averaged to improve the statistical robustness of each estimate. The microSWIFT spectra thus have a minimum of 51 degrees of freedom, which is comparable to the AWAC spectral estimates with 48 degrees of freedom. These spectral characteristics result is a frequency resolution of 0.016 Hz. Each of the spectra computed from the microSWIFTs compares well with the spectra reported from the 4.5 m AWAC (Figure 7, Panel (c)). Since the microSWIFTs are at a different alongshore location

210   than the 4.5 m AWAC we expect some differences in the spectra. However, the strong agreement of each microSWIFT spectra and the AWAC validates that the sea surface elevation time series from the microSWIFTs is a valid measurement.

Computing stationary spectra from the sea surface elevation time series is not always possible since the water depth under the microSWIFTs is constantly changing as the microSWIFTs drift. Instead, the properties of the waves can be investigated using a zero-crossing algorithm, which identifies individual waves along the drift track of each microSWIFT. Here we define an

215   individual wave realization as the data between two consecutive upward zero-crossings in elevation. Since the microSWIFTs are spatially distributed in the nearshore and sampling simultaneously, some of the microSWIFTs will be measuring the same wave as it propagates passed multiple buoys. We treat this like 'sampling with replacement' method, which improves the robustness of the statistics by sampling many realizations. An example of processing Mission 19 using the zero-crossing approach is shown in Figure 8. Panel (a) shows the drift tracks of each microSWIFT over time while panel (b) shows that each

220   track is a different microSWIFT, each track is now a different color. Using the zero-crossing algorithm on each sea surface elevation time series (example in Figure 8, Panel (d)), we can define the height of each wave realization, from crest to trough, and the average location of the wave realization. The height of each wave realization is aggregated, and the distribution of wave heights sampled during this mission is shown in Figure 8, Panel (e). The distribution of wave heights follows a Rayleigh distribution as is expected for nearshore surface gravity waves Thornton and Guza (1983). The significant wave height is then

225 computed as the mean value of the top one-third largest waves in the distribution and is shown as a vertical line on the wave height distribution in Figure 8, Panel (e). We can also estimate the average location of each wave realization using the GPS location of the microSWIFT and the indices during each zero crossing interval. By applying this processing to each mission in the experiment, we get a total of 116,307 wave realizations across the experiment. We then find the average location of each wave realization that was measured by the microSWIFTs and look at the spatial distribution of the wave realizations (Figure

230 9). Most wave realizations were on the south side of the pier between -2 and -6 meters in bottom elevation. Using the locations of the wave realizations, the measured bathymetry, and the water level gauge, we can approximate the depth of each wave realization across the experiment.

We evaluate this zero-crossing processing method by again comparing computed values to the 4.5 m AWAC. We first find, for each mission, all wave realizations that had an average depth between -4.3 and -5.3 meters in bottom elevation. With this

235 subset of waves, we compute the significant wave height as the mean of the third-largest waves in the distribution. To calculate a significant wave height from one of these subsets of data, we require at least 30 wave realizations in the distribution. Thus, we do not compute a significant wave height for every mission. We compare the computed significant wave heights to those from the 4.5 m AWAC (Figure 10). Panel (a) shows that the time series of significant wave height from the 4.5 m AWAC and the estimates from the microSWIFT arrays qualitatively agree. Panel (b) directly compares the significant wave heights

240 between the 4.5 m AWAC and the microSWIFT arrays. The linear regression between the 4.5 m AWAC and microSWIFT array significant wave heights has a slope of 1.08 and an R^2 value of 0.67, showing a strong correlation between the two significant wave height estimates. This agreement is reasonable given that the microSWIFTs are measuring at a different alongshore location than the AWAC, although in similar water depths. We also expect that the microSWIFT arrays may under-predict some significant wave heights as the sampling windows are shorter than the AWAC, potentially not measuring the largest and

245 least likely waves in the distribution. Nevertheless, the strong agreement in significant wave height and scalar energy density spectra supports that the microSWIFT data are robust and suitable for investigating the dynamics of nearshore waves in both a statistical and wave-by-wave framework.

4 Data and Code Availability

The data from the DUNEX experiment are available at https://doi.org/10.5061/dryad.hx3ffbgk0 (Rainville et al., 2023). The

250 dataset consists of netCDF files for each mission, totaling 68 files after all data processing and cleaning. Each netCDF file contains metadata on the mission, including the people who worked on the deployments, deployment style, and Level 1 and Level 2 data, along with all associated metadata. The code used to process the Level 0 data to Level 1 and 2 data and to build the final dataset is stored in a GitHub repository at https://github.com/SASlabgroup/DUNEXMainExp. The code used to analyze the data is also contained in the same repository and can be used as an example code to start future analyses.

5 Conclusions

We created a unique dataset of measurements of surface gravity waves and surface currents in the inner shelf and surf zone by using large, coherent arrays of microSWIFT wave buoys. The processing of the raw, Level 0, data from the microSWIFT wave buoys involves a correction of directly measured accelerations from the body frame of reference to the Earth frame of reference (NED reference frame) by applying a 9 degrees-of-freedom indirect Kalman filter, followed by band-pass filtering and integrating the signals to Level 2 data products. We have evaluated individual microSWIFT buoys through comparisons of estimates of spectral energy density and significant wave height with estimates from a nearby fixed acoustic wave and currents sensor. We then used a zero crossing algorithm on the time series of sea surface elevation from each microSWIFT to extract individual realizations of measured waves in the field. By aggregating the realizations of waves across each microSWIFT on a mission, we get a robust estimate of the significant wave height compared to that of the nearby acoustic waves and currents sensor. The coherent arrays provide high spatial and temporal resolution measurements during each deployment. We can use these data to investigate surface waves and currents in a bulk statistical sense and also in a wave-by-wave framework. Over the experiment, we deployed 81 arrays ranging from 2 to 50 microSWIFTs. Post-data cleaning left 68 complete missions across the dataset. These 68 missions resulted in a total of 116,307 wave realizations. These data will be used to investigate nearshore wave dynamics and surface circulation patterns and act as a validation dataset for wave-averaged and wave-resolving numerical models.

Author contributions. All authors participated in the data collection, analysis, and writing. Rainville developed the analysis software and prepared the archival dataset. Thomson, Moulton, and Derakhti conceived of the original project and obtained the funding.

Competing interests. The authors declare that they have no conflict of interest.

Acknowledgements. This work was completed as part of the During Nearshore Event Experiment (DUNEX), which was facilitated by the U.S. Coastal Research Program (USCRP). We thank USCRP for their support of this effort through funding for logistics and coordination (W912HZ-19-2-0045). We would like to thank field engineers Alex de Klerk, Joe Talbert, Emily Iseley, and Nate Clemmet for their efforts in designing, manufacturing, and deploying the microSWIFTs. We also thank Christine Baker, Emma Nuss, Sean McGill, and Jacob Davis for their support in the field. We thank the Town of Duck surf rescue for their help in deploying and retrieving the microSWIFTs throughout the field experiment. We also thank the U.S. Army Engineer Research and Development Center's Field Research Facility for the use of their facility and support staff. We would like to specifically thank Patrick Dickhudt, Mike Forte, Spicer Bak, and many others at the field research facility for all the help they provided in collection and publication of these data.

References

Bertin, X.: Storm surges and coastal flooding: status and challenges, La Houille Blanche, 102, 64–70, https://doi.org/10.1051/lhb/2016020, 2016.

Boehm, A. B., Ismail, N. S., Sassoubre, L. M., and Andruszkiewicz, E. A.: Oceans in Peril: Grand Challenges in Applied Water Quality Research for the 21st Century, Environmental Engineering Science, 34, 3–15, https://doi.org/10.1089/ees.2015.0252, 2017.

Booij, N., Holthuijsen, L. H., and Ris, R. C.: THE "SWAN" WAVE MODEL FOR SHALLOW WATER, Coastal Engineering Proceedings, https://doi.org/10.9753/icce.v25, number: 25, 1996.

Brown, A., Thomson, J., Ellenson, A., Rollano, F. T., Ozkan-Haller, H. T., and Haller, M. C.: Kinematics and Statistics of Breaking Waves Observed Using SWIFT Buoys, IEEE Journal of Oceanic Engineering, 44, 1011–1023, https://doi.org/10.1109/JOE.2018.2868335, 2019.

Derakhti, M., Kirby, J. T., Shi, F., and Ma, G.: Wave breaking in the surf zone and deep-water in a non-hydrostatic RANS model. Part 1: Organized wave motions, Ocean Modelling, 107, 125–138, https://doi.org/10.1016/j.ocemod.2016.09.001, 2016a.

Derakhti, M., Kirby, J. T., Shi, F., and Ma, G.: Wave breaking in the surf zone and deep-water in a non-hydrostatic RANS model. Part 2: Turbulence and mean circulation, Ocean Modelling, 107, 139–150, https://doi.org/10.1016/j.ocemod.2016.09.011, 2016b.

Elgar, S., Guza, R. T., Raubenheimer, B., Herbers, T. H. C., and Gallagher, E. L.: Spectral evolution of shoaling and breaking waves on a barred beach, Journal of Geophysical Research: Oceans, 102, https://doi.org/10.1029/97JC01010, 1997.

Feddersen, F., Guza, R. T., Elgar, S., and Herbers, T. H. C.: Alongshore momentum balances in the nearshore, Journal of Geophysical Research: Oceans, 103, https://doi.org/10.1029/98JC01270, 1998.

Gallagher, E. L., Elgar, S., and Guza, R. T.: Observations of sand bar evolution on a natural beach, Journal of Geophysical Research: Oceans, 103, 3203–3215, https://doi.org/10.1029/97JC02765, 1998.

Gomes, E. R., Mulligan, R. P., Brodie, K. L., and McNinch, J. E.: Bathymetric control on the spatial distribution of wave breaking in the surf zone of a natural beach, Coastal Engineering, 116, 180–194, https://doi.org/10.1016/j.coastaleng.2016.06.012, 2016.

Herbers, T. H. C., Jessen, P. F., Janssen, T. T., Colbert, D. B., and MacMahan, J. H.: Observing Ocean Surface Waves with GPS-Tracked Buoys, Journal of Atmospheric and Oceanic Technology, 29, 944–959, https://doi.org/10.1175/JTECH-D-11-00128.1, 2012.

Intergovernmental Panel on Climate Change: Climate Change 2021 - The Physical Science Basis - Summary for Policymakers, https://www.ipcc.ch/report/sixth-assessment-report-working-group-i/, 2021.

Karim, S. A. A., Rosli, M. A. M., and Mustafa, M. I. M.: Cubic spline interpolation for petroleum engineering data, Applied Mathematical Sciences, 8, 5083–5098, https://doi.org/10.12988/ams.2014.44284, 2014.

Kirby, J. T., Wei, G., Chen, Q., Kennedy, A. B., and Dalrymple, R. A.: Funwave 1.0: Fully Nonlinear Boussinesq Wave Model - Documentation and User's Manual, research report NO. CACR-98-06, https://repository.tudelft.nl/islandora/object/uuid%3Ad79bba08-8d35-47e2-b901-881c86985ce4, 1998.

Kuik, A. J., Vledder, G. P. v., and Holthuijsen, L. H.: A Method for the Routine Analysis of Pitch-and-Roll Buoy Wave Data, Journal of Physical Oceanography, 18, 1020–1034, https://doi.org/10.1175/1520-0485(1988)018<1020:AMFTRA>2.0.CO;2, 1988.

Ma, G., Shi, F., and Kirby, J. T.: Shock-capturing non-hydrostatic model for fully dispersive surface wave processes, Ocean Modelling, 43-44, 22–35, https://doi.org/10.1016/j.ocemod.2011.12.002, 2012.

Martínez, M. L., Intralawan, A., Vázquez, G., Pérez-Maqueo, O., Sutton, P., and Landgrave, R.: The coasts of our world: Ecological, economic and social importance, Ecological Economics, 63, 254–272, https://doi.org/10.1016/j.ecolecon.2006.10.022, 2007.

Neumann, J. E., Emanuel, K., Ravela, S., Ludwig, L., Kirshen, P., Bosma, K., and Martinich, J.: Joint effects of storm surge and sea-level rise on US Coasts: new economic estimates of impacts, adaptation, and benefits of mitigation policy, Climatic Change, 129, 337–349, https://doi.org/10.1007/s10584-014-1304-z, 2015.

Pedersen, T., Siegel, E., and Wood, J.: Directional Wave Measurements from a Subsurface Buoy with an Acoustic Wave and Current Profiler (AWAC), in: OCEANS 2007, pp. 1–10, https://doi.org/10.1109/OCEANS.2007.4449153, 2007.

Raghukumar, K., Chang, G., Spada, F., Jones, C., Janssen, T., and Gans, A.: Performance Characteristics of "Spotter," a Newly Developed Real-Time Wave Measurement Buoy, Journal of Atmospheric and Oceanic Technology, 36, 1127–1141, https://doi.org/10.1175/JTECH-D-18-0151.1, 2019.

Rainville, E. J., Thomson, J., Moulton, M., and Derakhti, M.: Measurements of Nearshore Waves through Coherent Arrays of Small-Scale, Free-Drifting Wave Buoys, 2022.

Rainville, E. J., Thomson, J., Moulton, M., and Derakhti, M.: Measurements of Nearshore Waves through Coherent Arrays of Free-Drifting Wave Buoys (UW_drifters), https://doi.org/doi:10.5061/dryad.hx3ffbgk0, 2023.

Ruessink, B. G., Miles, J. R., Feddersen, F., Guza, R. T., and Elgar, S.: Modeling the alongshore current on barred beaches, Journal of Geophysical Research: Oceans, 106, 22 451–22 463, https://doi.org/10.1029/2000JC000766, 2001.

Schmidt, W. E., Woodward, B. T., Millikan, K. S., Guza, R. T., Raubenheimer, B., and Elgar, S.: A GPS-Tracked Surf Zone Drifter, Journal of Atmospheric and Oceanic Technology, 20, 1069–1075, https://doi.org/10.1175/1460.1, 2003.

Schmidt, W. E., Guza, R. T., and Slinn, D. N.: Surf zone currents over irregular bathymetry: Drifter observations and numerical simulations, Journal of Geophysical Research, 110, C12 015, https://doi.org/10.1029/2004JC002421, 2005.

Shi, F., Kirby, J. T., Harris, J. C., Geiman, J. D., and Grilli, S. T.: A high-order adaptive time-stepping TVD solver for Boussinesq modeling of breaking waves and coastal inundation, Ocean Modelling, 43, 36–51, 2012.

Spydell, M., Feddersen, F., Guza, R. T., and Schmidt, W. E.: Observing Surf-Zone Dispersion with Drifters, Journal of Physical Oceanography, 37, 2920–2939, https://doi.org/10.1175/2007JPO3580.1, 2007.

Svendsen, I. A.: Introduction To Nearshore Hydrodynamics, World Scientific Publishing Company, 2005.

Thomson, J.: Wave Breaking Dissipation Observed with "SWIFT" Drifters, Journal of Atmospheric and Oceanic Technology, 29, 1866–1882, https://doi.org/10.1175/JTECH-D-12-00018.1, 2012.

Thomson, J., Schwendeman, M. S., Zippel, S. F., Moghimi, S., Gemmrich, J., and Rogers, W. E.: Wave-Breaking Turbulence in the Ocean Surface Layer, Journal of Physical Oceanography, 46, 1857–1870, https://doi.org/10.1175/JPO-D-15-0130.1, 2016.

Thomson, J., Girton, J. B., Jha, R., and Trapani, A.: Measurements of Directional Wave Spectra and Wind Stress from a Wave Glider Autonomous Surface Vehicle, Journal of Atmospheric and Oceanic Technology, 35, 347–363, https://doi.org/10.1175/JTECH-D-17-0091.1, 2018.

Thornton, E. B. and Guza, R. T.: Transformation of wave height distribution, Journal of Geophysical Research: Oceans, 88, 5925–5938, https://doi.org/10.1029/JC088iC10p05925, 1983.

Tolman, H. L.: User manual and system documentation of WAVEWATCH III TM version 3.14, 1999.

Voermans, J. J., Babanin, A. V., Thomson, J., Smith, M. M., and Shen, H. H.: Wave Attenuation by Sea Ice Turbulence, Geophysical Research Letters, 46, 6796–6803, https://doi.org/10.1029/2019GL082945, 2019.

Zippel, S. and Thomson, J.: Surface wave breaking over sheared currents: Observations from the Mouth of the Columbia River, Journal of Geophysical Research: Oceans, 122, 3311–3328, https://doi.org/10.1002/2016JC012498, 2017.
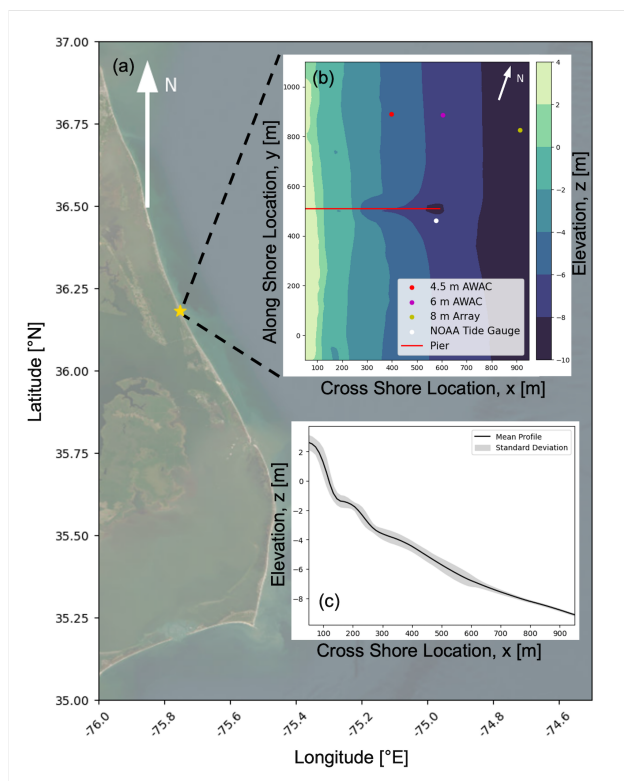
Figure 1. (a) Aerial imagery of the Outer Banks of North Carolina, US where the gold star is the location of the US Army Corps of Engineers - Field Research Facility (FRF) (© Source: Esri, Maxar, Earthstar Geographics, and the GIS User Community). Panel (b) shows the bathymetry contours at the field site from October 21st, 2021 relative to the NAVD88 datum and locations of fixed instrumentation (Data provided by USACE, Field Research Facility, https://frfdataportal.erdc.dren.mil/). Panel (c) shows the average cross-shore profile of the bathymetry with one standard deviation above and below the average.
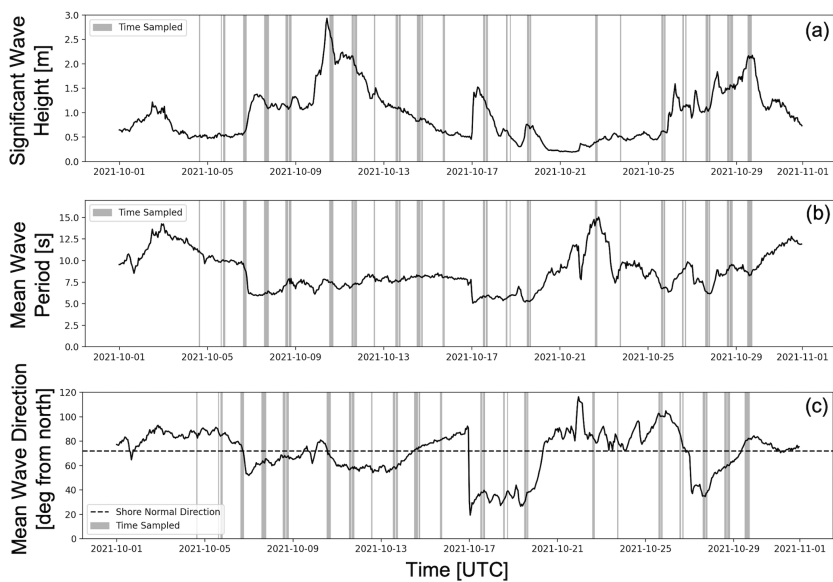
Figure 2. Conditions sampled during the main DUNEX experiment from the Field Research Facility 8 m array. Time series of the (a) significant wave height and (b) mean wave period and (c) mean wave direction (Data provided by USACE, Field Research Facility, https://frfdataportal.erdc.dren.mil/). The gray patches show the times that we deployed microSWIFT arrays.
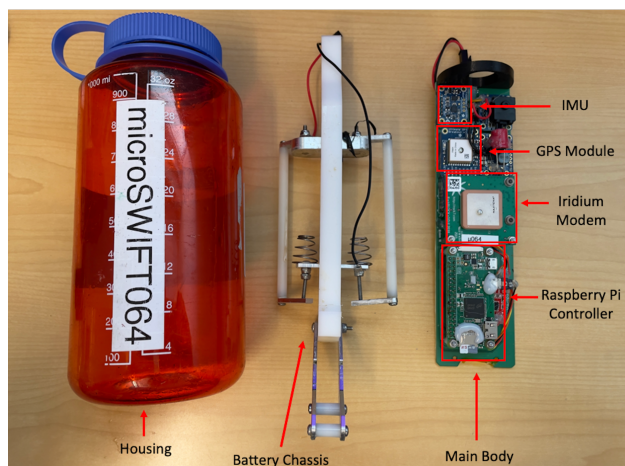
Figure 3. Layout of microSWIFT hardware components with the Nalgene water bottle housing on the far left, battery chassis in the middle and the electronics on the far right. The individual chipsets include a Raspberry Pi Zero as the main processor, a GPS module, inertial measurement unit(IMU) that contains accelerometers, gyroscopes, and magnetometers, and an iridium modem.
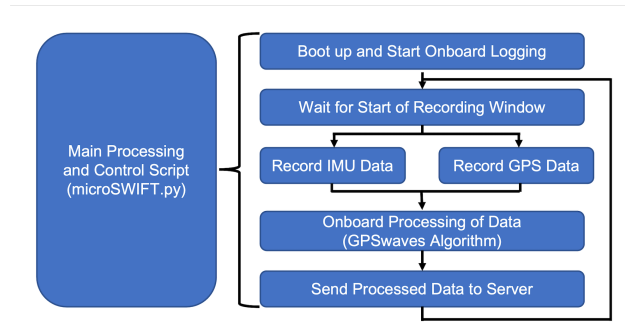
Figure 4. Flow of operations for software onboard the microSWIFT wave buoys.
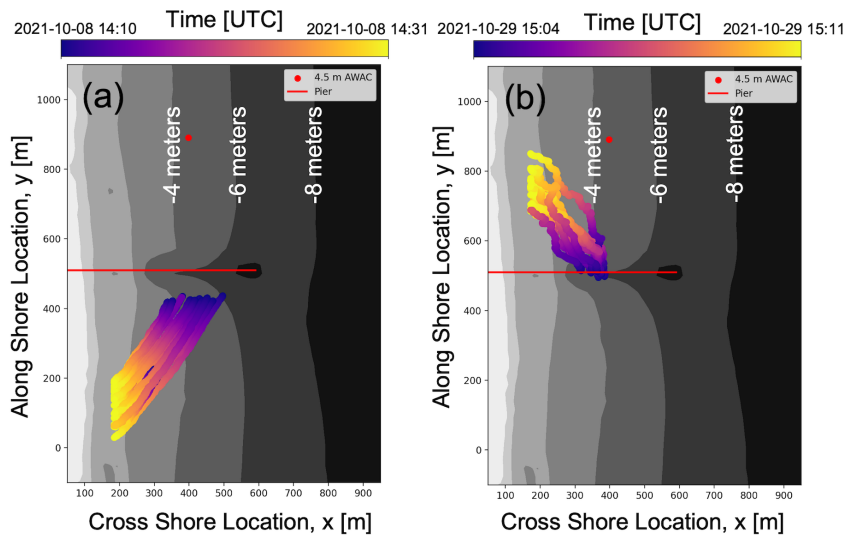
Figure 5. Example drift tracks(location of microSWIFTs over time) of microSWIFT arrays during a mission plotted over of the bathymetry digital elevation model shown in Figure 1 Panel (b). Panel (a) shows the drift tracks from mission 16 which has 19 microSWIFTs deployed and Panel (b) shows the drift tracks from mission 79 which has 13 microSWIFTs deployed.
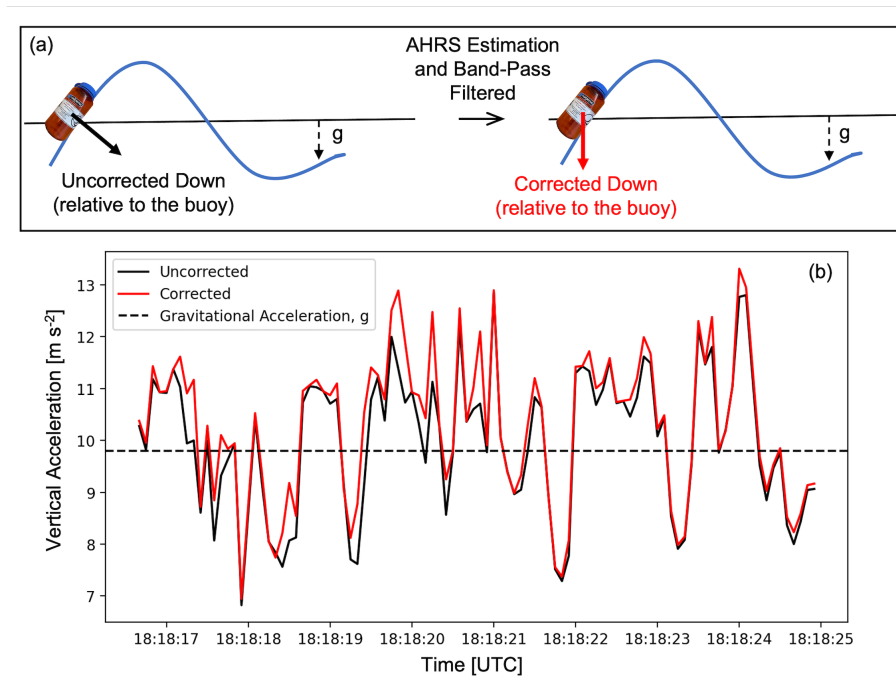
Figure 6. Panel (a) shows a schematic representation of the acceleration corrections from the body reference frame of the microSWIFT to the Earth reference frame through the use of the attitude and heading reference system (AHRS) estimation and band-pass filtering. Panel (b) shows an example portion of a signal to see how the vertical acceleration is corrected.
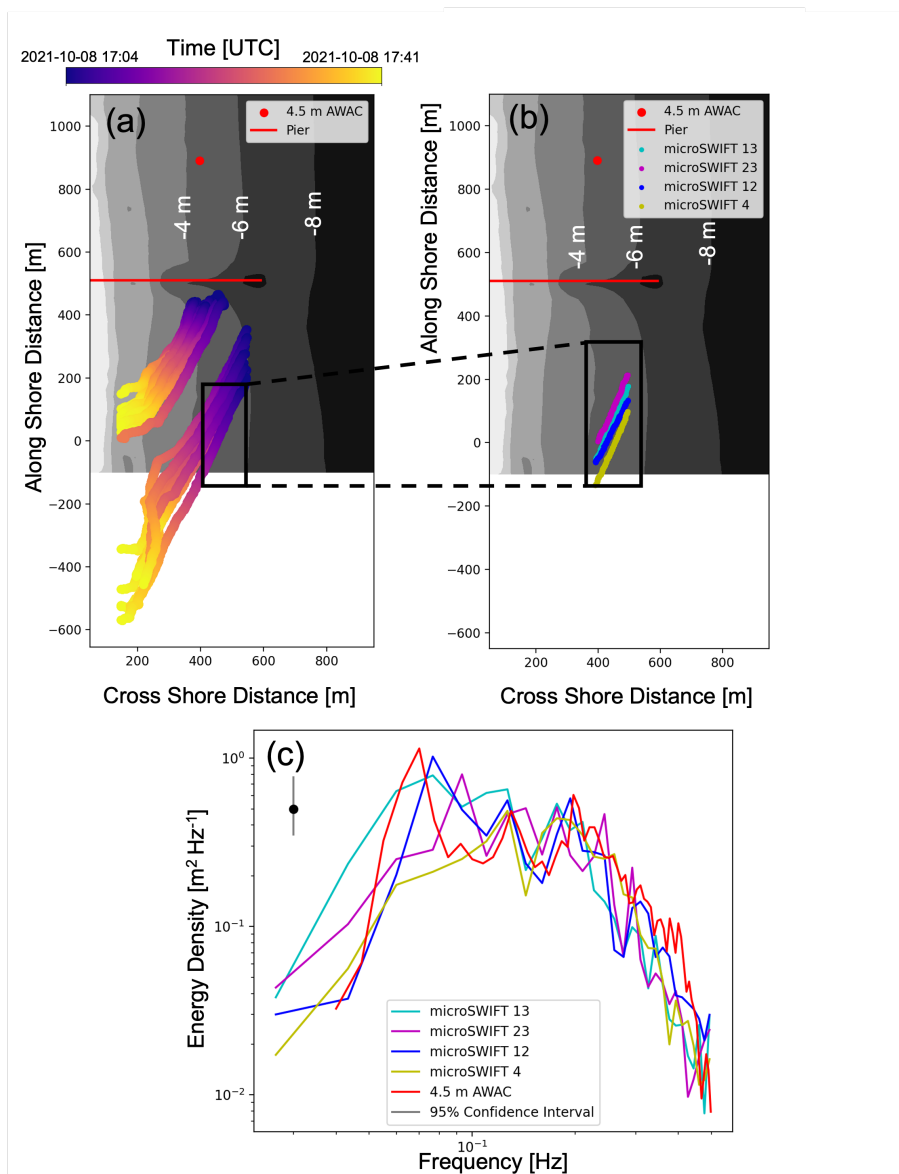
Figure 7. Comparisons of Panel (a) shows the drift tracks of the microSWIFTs from mission 18 plotted over the surveyed bathymetry DEM. Panel (b) is showing a subset of the drift tracks where the bathymetry along each track is between -4.3 and -5.3 meters and each microSWIFT as a different color. Panel (c) shows the spectra computed from subset of the sea surface elevation time series for each microSWIFT. One error bar is shown for the largest confidence interval of the spectra with 51 degrees of freedom.
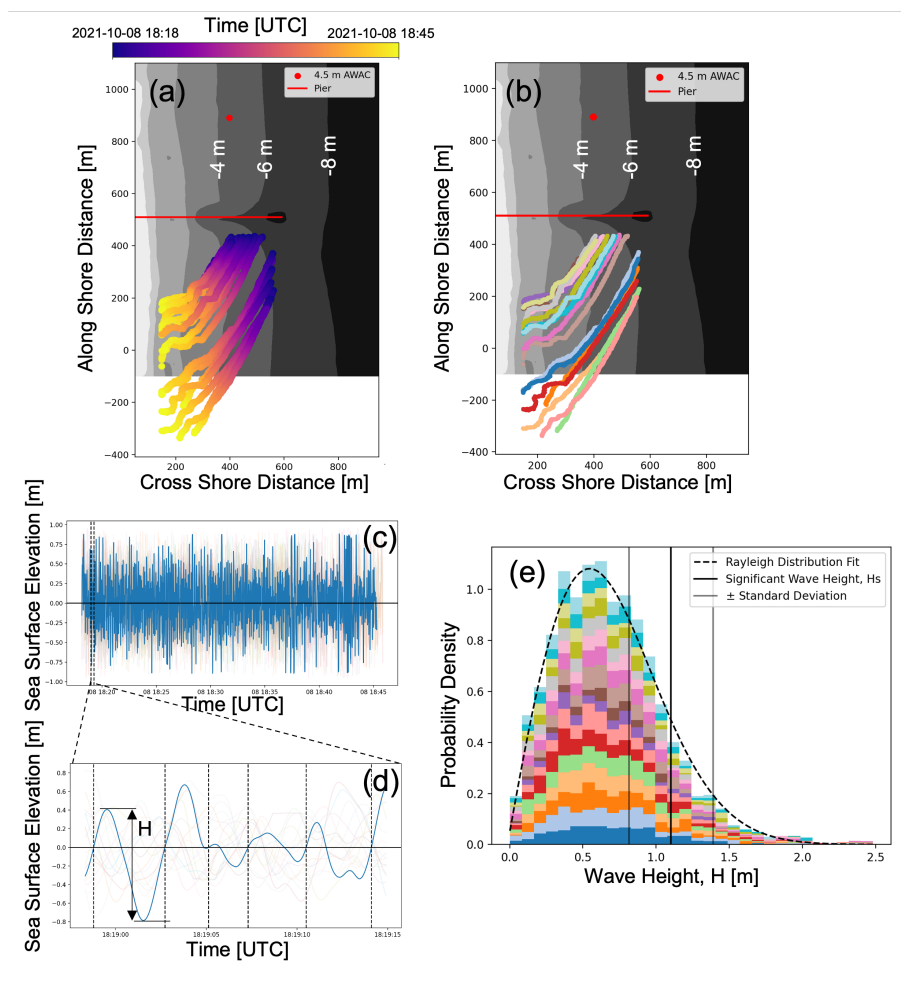
Figure 8. Example of steps in processing each mission. Panel (a) shows the drift tracks of the microSWIFTs from mission 19 plotted over the surveyed bathymetry DEM. Panel (b) is showing the same drift tracks as Panel (a) but showing each microSWIFT as a different color. Panel (c) show the time series of computed sea surface elevation with one time series being highlighted as an example. Panel (d) is a zoomed in portion of the over all time series showing the locations of zero crossings and how we define the height of an individual wave in a time series. Panel (e) is the probability density of all wave heights from the entire time series where the colors are showing the contribution from each microSWIFT with the corresponding color. The probability density distribution fits a Rayleigh distribution. The vertical line shows the computed significant wave height for this distribution.
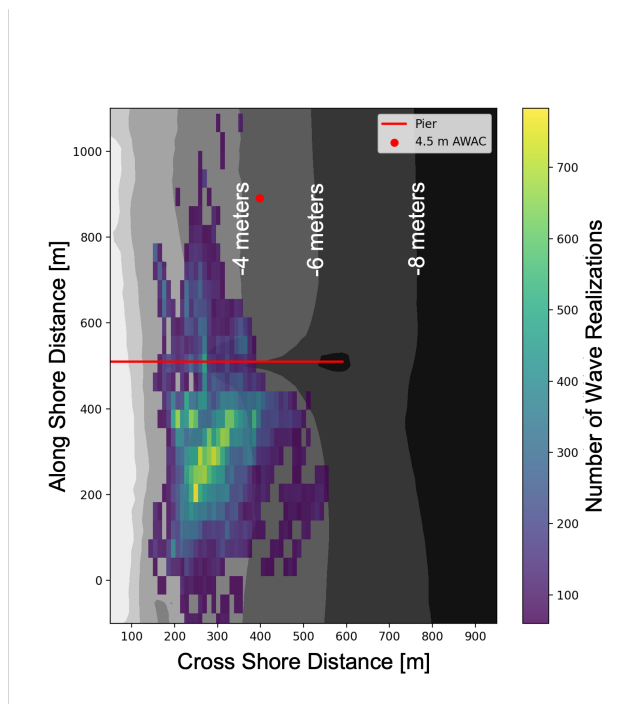
Figure 9. Number and location of wave realizations measured between October 3rd and October 30th, 2021 plotted over the bathymetry contours. Most wave realizations were measured on the south side of the pier between -2 and -6 meters in bottom elevation. The bin spacing for this histogram is 10.5 meter bins in the cross shore direction and 43 meter bins in the along shore direction.
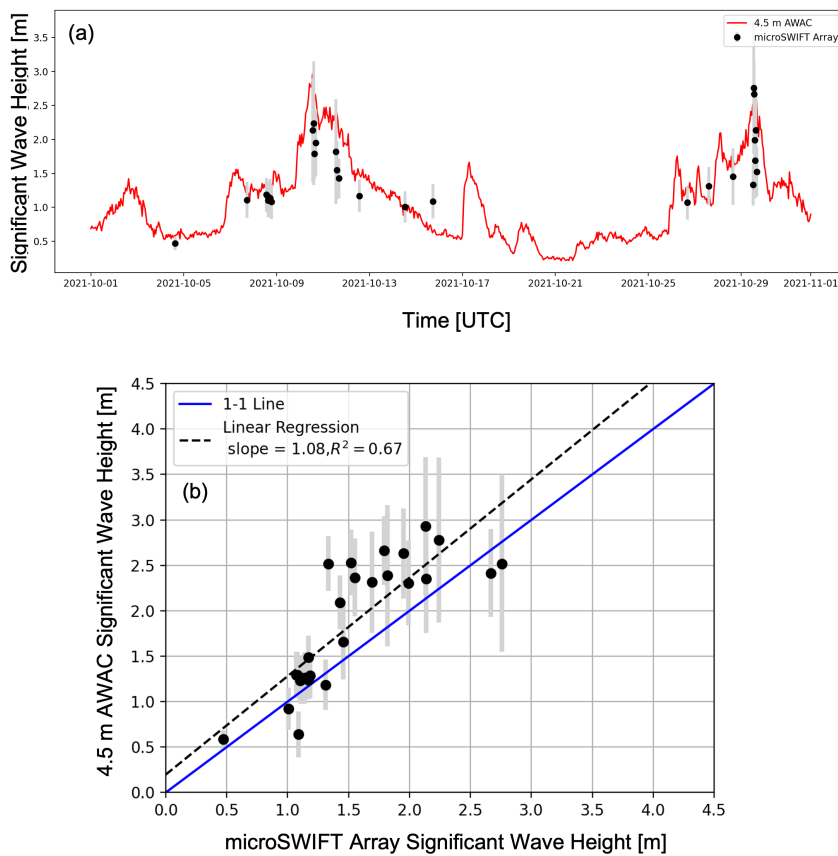
Figure 10. Comparison of the estimated significant waves heights from the microSWIFT arrays to the estimates from the 4.5 m AWAC. While the microSWIFT arrays are not in the same water depth as the 4.5 m AWAC we see that the microSWIFT array characterizes the size of the waves with good comparison to the 4.5 m AWAC. The gray bars indicate error bars (± 1 standard deviation of the top third largest wave heights) around each of the significant wave height estimates.

Sensor	Chipset	Sensitivity	Range	Average Noise Variance
3-axis Linear Accelerometer	FXOS8700CQ	$0.244\ mg\ LSB^{-1}$ $0.488\ mg\ LSB^{-1}$	$\pm 2g$ / $\pm 4g$	$0.00004\ m\ s^{-2}$
3-axis Magnetometer	FXOS8700CQ	$0.1\ \mu T\ LSB^{-1}$	$\pm\ 1200\ \mu T$	$2\ \mu T$
3-axis Gryoscope	FXAS21002C	15.625 $mdps\ LSB^{-1}$	$\pm\ 500\ dps$	$0.045\ dps$

Table 1. Inertial Measurement Unit sensor specifications for accelerometer, gyroscope and magnetometer onboard each microSWIFT. Note that the dynamic range of the accelerometer was adjusted from 2g to 4g part way through the field experiment on Mission 53 on October 23rd, 2021.